PHYSICAL REVIEW B VOLUME 39, NUMBER 10 1 APRIL 1989

Microstructure, lattice parameters, and superconductivity of $YBa_2(Cu_{1-x}Fe_x)_3O_{7-\delta}$ for $0 \leq x \leq 0.33$

Youwen Xu, M. Suenaga, J. Tafto,[*] R. L. Sabatini, and A. R. Moodenbaugh
Department of Applied Science, Brookhaven National Laboratory, Upton, New York 11973

P. Zolliker
Department of Physics, Brookhaven National Laboratory, Upton, New York 11973

(Received 14 November 1988)

Iron was substituted for copper in $YBa_2(Cu_{1-x}Fe_x)_3O_{7-\delta}$ for $0 \leq x \leq 0.33$. Superconducting transition temperatures and lattice parameters have been determined as a function of Fe content. The orthorhombic distortion $\Delta a_0 = 2(b-a)/(a+b)$ decreased to zero near $x = 0.03$. Beyond $x = 0.03$ the structure appears tetragonal. For compositions $0 \leq x \leq 0.15$ the superconducting critical temperature T_c decreased smoothly from $T_c = 90$ K to below 4.2 K. Transmission electron microscopy (TEM) revealed that the spacing between the twin boundaries decreased from ~ 200 nm for $x = 0$ to ~ 20 nm for $x = 0.02$ before the twins disappeared for $x \gtrsim 0.03$. The sharp streaks in TEM diffraction patterns were interpreted as due to the twin boundary layers whose thickness varied from ~ 1 nm for the pure to ~ 2 for the Fe ($x = 0.02$) containing specimen. A tweed structure in the TEM image and associated diffuse streaks along the $\langle 110 \rangle$ directions in electron diffraction pattern appeared for $x > 0.015$. This observation suggests that the structure consists of fine (< 5 nm) orthorhombic domains, each domain having the twinlike crystallographic relation with its neighbors. Rietveld refinement of powder neutron diffraction for $x = 0.10$ and 0.167 determined that Fe substituted primarily on the Cu "chain" site, and for every two atoms of Fe substituted, approximately one extra oxygen is incorporated in the Cu-O plane.

I. INTRODUCTION

Superconducting $YBa_2Cu_2O_7$ (1:2:3), discovered by Wu *et al.*,[1] has been extensively studied. Replacement of Y by other rare-earth elements does not change the superconducting properties of the compounds even when the rare-earth element carries a large magnetic moment.[2-4] Cu is assumed to play an important role in these superconductors since CuO_2 planes are common to the superconductors containing La, Y, Bi, and Tl. In $YBa_2Cu_2O_7$ there are two distinct sites for Cu, one forming CuO_2 planes, the other forming CuO chains. Replacement of Cu by other transition metals may provide information about the nature of superconductivity in this compound. If the transition metal substitutes for Cu preferentially on either one of the two sites, then that fact could be used to determine the relative importance of these two distinct Cu sites for superconductivity.

$YBa_2Cu_3O_{7-\delta}$ undergoes a structural phase transition from tetragonal to orthorhombic (T-O) when temperature is lowered below 700 °C as oxygen is taken into the sample.[5] At the same time, twins form due to the strain associated with the phase transformation. The effect of twins on superconductivity of this ceramic superconductor has been a topic of speculation for both theorists and experimentalists. One of the motivations for this work is to investigate the role of twin boundaries on superconducting properties of the high-T_c oxide. There is a variety of theories about the effect of twin boundaries on the superconducting properties of $YBa_2Cu_3O_7$. Fang *et al.*[6] proposed the twin boundary region has higher T_c than the matrix. If this is the case the effect should be observable for the spacing less than 10–20 nm. Mueller *et al.*[7] assumed that the twin boundaries play an important role in high-T_c oxides. Chaudhari[8] suggested that twin boundaries act as strong flux pinning centers which result in higher critical current in thin films. Deutscher and Müller[9] proposed that twin boundaries are nonorthorhombic and nonsuperconducting or weakly superconducting regions.

Much has been published[10-26] on the effect of Fe substitutions for Cu on superconducting properties. While sample preparation methods appear to dramatically affect superconducting properties, these reports generally find that T_c falls as Fe replaces Cu. However, except for that basic observation, there is little agreement on the details of the dependence of T_c on Fe content. Also, since Fe substitution results in a reduced $\Delta a_0[=2(b-a)/(a+b)]$ for $x < 0.03$ and a tetragonal phase for $x \gtrsim 0.03$,[10-12] one expects the twin-boundary spacings to change with Fe concentration. Thus, in order to study in detail the effect of the substitution on both superconducting properties and the microstructures, we substituted Fe for Cu to give the nominal compositions $YBa_2(Cu_{1-x}Fe_x)_3O_{7-\delta}$ with $0 \leq x \leq 0.33$. While x-ray and neutron-diffraction techniques indicate that beyond $x = 0.03$ the room-temperature structure is tetragonal (rather than orthorhombic), electron diffraction suggests the existence of mutually perpendicular microdomains of orthorhombic regions. Fe appears to be soluble up to near $x = 0.15$. We report changes in superconducting temperatures and in microstructure as a function of Fe content x in the compounds $YBa_2(Cu_{1-x}Fe_x)_3O_{7-\delta}$. Results from superconductivity measurements, electrical resistivity data, x-ray and neutron-diffraction studies, optical micrography to determine grain size and homogeneity, electron microprobe for composition, and transmission electron microscopy to study microstructural variations, give a comprehensive and consistent picture of the effects of Fe substitution for Cu.

The primary microstructural modifications occurring due to the Fe substitution are (1) reduction of the spacing between the twin boundaries for $x \leq 0.02$, (2) increase of the twin-boundary layer thickness with the Fe substitutions, (3) disappearance of the boundaries for $x \gtrsim 0.03$ and appearance of a "tweedlike" structure for $x \gtrsim 0.015$, and (4) disappearance of the tweed structure for $x \gtrsim 0.1$. Possible mechanisms for reduction of the twin spacing and formation of the tweedlike structure as well as the influence of these microstructural changes on superconducting properties are discussed in detail. A preliminary report on some of this work was reported earlier.[27]

Although this paper describes the microstructural changes of 1:2:3 oxides due to Fe substitution for Cu, it should be pointed out that similar changes are also observed when other elements are substituted for Cu, e.g., Ga,[10,11,28] Al,[10,29] and Co,[10,11,30] which are known to induce an orthorhombic-to-tetragonal phase transformation.

II. EXPERIMENTAL DETAILS

The samples were prepared by mixing the appropriate amounts of Y_2O_3, $BaCO_3$, CuO, and Fe_2O_3 powders in an agate mortar. In order to achieve the best results, the powders were ground thoroughly (40 min for a 5-g sample) before the first firing. The intermediate grindings were fast (about 15 min) to avoid possible effects of moisture in the atmosphere on the samples. The ground powders were pressed into pellets and fired in the air at 900 °C twice. Finally, they were heated in oxygen at 970 °C for more than 40 h, followed by an anneal at 665 °C for 8 h, and then furnace cooled to below 100 °C. The resulting samples were well crystalized with shiny facets on the interior. Some of the grains were as large as 200 μm in one direction for the pure $YBa_2Cu_2O_7$. An electron microprobe analysis was used to verify the composition of the samples. The results indicated that the final compositions of the oxides were very close to the nominal compositions for $x \leq 0.15$. For example, the Fe contents for $x = 0.05$ and 0.15 were measured to be $x = 0.049 \pm 0.002$ and 0.142 ± 0.006, respectively. X-ray powder-diffraction scans were taken with a conventional setup utilizing Cu $K\alpha$ radiation and a diffracted-beam monochromator. All samples with Fe content $x = 0$ to 0.15 showed no observable impurity peaks in the x-ray-diffraction pattern above the 2% level of detection.

Powder-neutron-diffraction measurements on 8-g samples with $x = 0.10$ and $x = 0.167$ were carried out on the triple-axis spectrometer H4S at the Brookhaven High Flux Beam Reactor (HFBR). The experimental configuration consisted of a pyrolytic graphite monochromator and analyzer in the (002) and (004) settings respectively, and the following collimation: 20′ in pile, 40′ monochromator sample, 40′ sample analyzer, and 20′ analyzer detector. The neutron wavelength was 0.2370(1) nm. A pyrolytic graphite filter was used to suppress higher-order wavelengths. The data for the sample with $x = 0.10$ was obtained at room temperature by step scanning at 0.1° intervals. The sample having $x = 0.167$ was mounted in a cryostat and cooled to 10 K for the diffraction measurements.

The superconducting transition temperature T_c was measured by mutual inductance, and the dc electrical resistivity was measured by the standard four-probe technique. The transmission electron microscopy was performed on a JEM-100C electron microscope operated at 120 keV.

The majority of the TEM specimen (at least two for each composition) were prepared by slicing sintered pellets, ultrasonically cutting out 3-mm disks, mechanically dimpling to ∼25 μm thick, initially ion milling at 4 kV at 8–10° tilt, and finally, milling at a reduced angle of ∼6° or reduced voltage of 2 kV. To verify that no artifacts were being introduced during the ion-milling process at room temperature, several specimens of ground pellets suspended on holey carbon films were examined, as well as samples ion milled using a liquid-nitrogen-cooled stage. The only observable differences among the specimens prepared by these various methods is that the ion-milled samples had a very thin amorphous layer on the surface.

III. RESULTS

A. X-ray diffraction

X-ray-diffraction patterns revealed systematic changes in lattice parameters as Fe content was varied. The detailed changes in peaks 006, 020, and 200 are illustrated in Fig. 1. For $x = 0.03$, the 200 and 020 have merged. A slight broadening of this peak relative to the 006 gives evidence that b is not yet quite equal to a. In fact, close inspection at the sample by TEM shows a small portion of the sample to be twinned (orthorhombic), the remainder free of twins (tetragonal). Thus, the composition $x = 0.03$ is apparently near the *T-O* boundary. Slight compositional inhomogeneity (Fe or O) in the specimens may explain the simultaneous presence of tetragonal and orthorhombic phases.

The lattice parameters of the samples were calculated by a least-squares fit to positions from the x-ray diffraction pattern with an internal silicon standard. The results are shown in Fig. 2 and listed in Table I. Since the symmetry of the structure is not known, we cannot state with certainty that the crystal structure is tetragonal even when a and b are equal for $x = 0.03$. This value of x for the *T-O* boundary is higher than those in published work, i.e., $x = 0.023$.[10,11] At Fe contents above $x = 0.03$, a increases slightly with x. Assuming that all or most of the Fe substitutes onto Cu(1) (chain site) atoms, the changes in a and b below $x = 0.03$ are probably caused by the disordering of the oxygen atoms due to random occupation of Fe on the Cu(1) site. The observed change in c for low

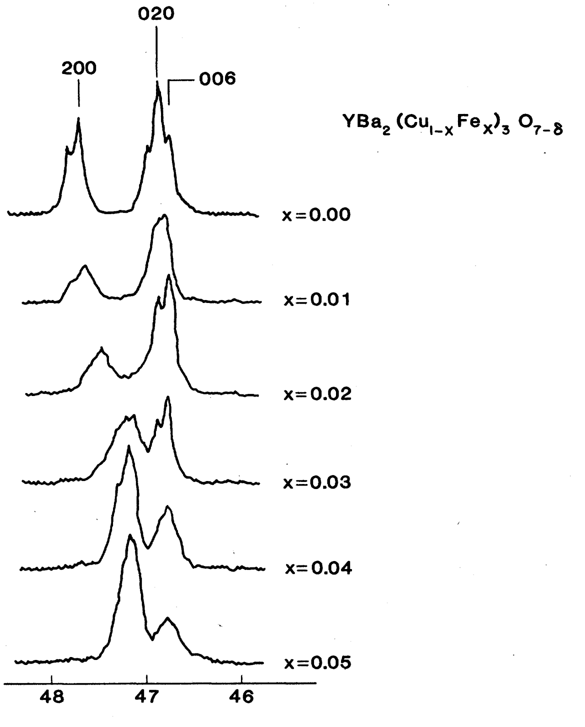

FIG. 1. X-ray powder-diffraction lines (200), (020), and (006) of $YBa_2(Cu_{1-x}Fe_x)_3O_{7-\delta}$ are shown for $x=0$, 0.01, 0.02, 0.03, 0.04, and 0.05 as a function of 2θ, $46° < 2\theta < 48°$.

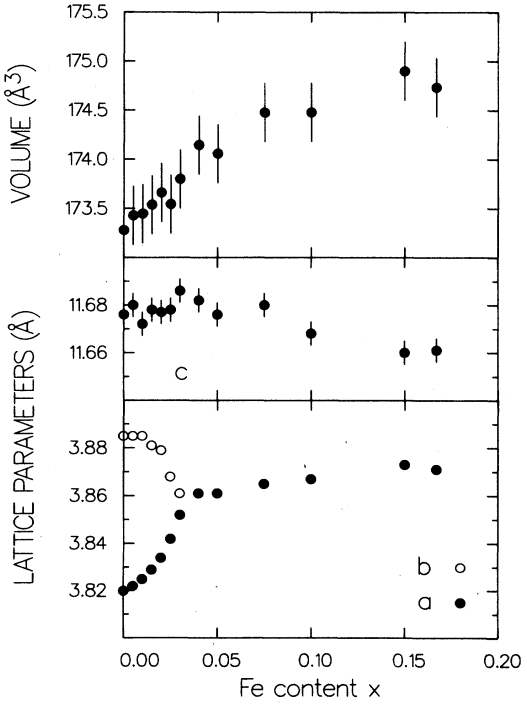

FIG. 2. The unit-cell volume and the lattice parameters of $YBa_2(Cu_{1-x}Fe_x)_3O_{7-\delta}$ as a function of the Fe content x as determined by x-ray powder diffraction.

TABLE I. Lattice parameters and unit-cell volumes of $YBa_2(Cu_{1-x}Fe_x)_3O_{7-\delta}$.

Fe ($x\times100\%$)	a (nm)	b (nm)	c (nm)	V (nm^3)
0.0	0.3820	0.3885	1.1676	0.173280
0.5	0.3822	0.3885	1.1680	0.173430
1.0	0.3825	0.3885	1.1672	0.173447
1.5	0.3829	0.3881	1.1678	0.173539
2.0	0.3834	0.3879	1.1677	0.173661
2.5	0.3842	0.3868	1.1678	0.173545
3.0	0.3852	0.3861	1.1686	0.173800
4.0	0.3861		1.1682	0.174147
5.0	0.3861		1.1676	0.174057
7.5	0.3865		1.1680	0.174478
10.0	0.3865		1.1668	0.174479
15.0	0.3873		1.1660	0.174901
16.7	0.3871		1.1661	0.174735
33.3	0.3866		1.1660	0.174269

substitution ($x < 0.03$) is of the same magnitude as the uncertainty of our parameter determination. At higher Fe content ($x > 0.05$), c decreases slightly. This is different from the case of the orthorhombic-to-the tetragonal phase change due to oxygen deficiency, where c monotonically increases with decreasing oxygen content. The overall volume of the unit-cell lattice increases as more Fe is substituted for Cu.

A specimen with nominal Fe content $x=0.33$ showed a significant amount of a second phase ($BaFeO_3$) and lattice parameters similar to those of the sample with $x=0.15$ as shown in Table I. Both of these observations suggest that, at least with our preparation methods, the solubility limit of Fe is approximately $x=0.15$.

The lattice parameters of our samples are basically in agreement with published work.[10,11,13] The relatively higher c we observed for higher Fe content may possibly be due to relatively higher oxygen content in our samples.

B. Neutron diffraction for $x=0.10$ and $x=0.167$

Structure refinements on the specimens $x=0.10$ and 0.167 were carried out with a local version of the Rietveld-Hewat program.[31,32] The peaks, assumed to be Gaussian with a small Lorentzian component to the peak profile, were described in the pseudo-Voigtian approximation, and the background was refined together with the structure. In the case of the $x=0.167$ specimen, diffraction peaks from the aluminum specimen holder were excluded from consideration. The diffraction data were indexed on a tetragonal cell with no systematic absences (space group $P4/mmm$). A few peaks, all smaller than 1% of the most intense peak, could not be indexed with this cell and were excluded from the refinement. The structure of $YBa_2Cu_2CoO_{7-\delta}$ (Ref. 33) was used as a starting model, using Fe instead of Co. The overall Fe composition was restricted to the nominal composition and the occupancies of the O(1) and O(2) sites were set to one. Significant improvement of the refinements were ob-

TABLE II. Crystal structure of $YBa_2Cu_{2.7}Fe_{0.3}O_{7.15}$ and $YBa_2Cu_{2.5}Fe_{0.5}O_{7.23}$.

$YBa_2Cu_{2.7}Fe_{0.3}O_{7.15}$ (295 K), space group: *P*4/*mmm*

		x	y	z	$B(10^{-2}\ nm^2)$	N^a
Y	in 1*d*	$\frac{1}{2}$	$\frac{1}{2}$	$\frac{1}{2}$	0.2(1)	1.0
Ba	in 2*h*	$\frac{1}{2}$	$\frac{1}{2}$	0.1863(3)	0.3(1)	2.0
Cu1	in 1*a*	0	0	0	0.3(2)^b	0.74(4)^b
Fe1	in 1*a*	0	0	0	0.3(2)^b	0.26(4)^b
Cu2	in 2*g*	0	0	0.3565(2)^b	0.1(2)^b	1.96(4)^b
Fe2	in 2*g*	0	0	0.3565(2)	0.1(2)^b	0.04(4)^b
O1	in 2*g*	0	0	0.1576(5)^b	1.3(2)	2.0
O2	in 4*i*	0	$\frac{1}{2}$	0.3781(3)	0.3(1)	4.0
O3	in 4*n*	0.044(6)	$\frac{1}{2}$	0	1.9(4)	1.15(3)

Unit cell^c (nm): $a=0.38655(15)$, $c=1.1674(5)$.
Agreement factors:^{d} $R_I=0.055$, $R_{wp}=0.081$, $S_p^2=1.6$, $S_I^2=3.8$.

$YBa_2Cu_{2.5}Fe_{0.5}O_{7.23}$ (10 K), space group: *P*4/*mmm*

		x	y	z	$B(10^{-2}\ nm^2)$	N^a
Y	in 1*d*	$\frac{1}{2}$	$\frac{1}{2}$	$\frac{1}{2}$	0.2(1)	1.0
Ba	in 2*h*	$\frac{1}{2}$	$\frac{1}{2}$	0.1849(4)	0.2(1)	2.0
Cu1	in 1*a*	0	0	0	0.5(2)^b	0.58(5)^b
Fe1	in 1*a*	0	0	0	0.5(2)^b	0.42(5)^b
Cu2	in 2*g*	0	0	0.3562(2)^b	0.0(2)^b	1.93(5)^b
Fe2	in 2*g*	0	0	0.3562(2)	0.0(2)^b	0.07(5)^b
O1	in 2*g*	0	0	0.1588(4)^b	0.5(2)	2.0
O2	in 4*i*	0	$\frac{1}{2}$	0.3781(3)	0.3(1)	4.0
O3	in 4*n*	0.037(9)	$\frac{1}{2}$	0	0.9(5)	1.23(3)

Unit cell^c (nm): $a=0.38505(15)$, $c=1.1576(5)$.
Agreement factors:^{d} $R_I=0.058$, $R_{wp}=0.088$, $S_p^2=1.4$, $S_I^2=3.9$.

[a] Number of atoms per formula unit.

[b] Constraint parameters: $B_{Cu_1}=B_{Fe_1}$, $B_{Cu_2}=B_{Fe_2}$, $N_{Cu_1}=1.0-N_{Fe_1}$, $N_{Fe_2}=0.3-N_{Fe_1}$, $N_{Cu_2}=1.7+N_{Fe_1}$, $z_{Cu_2}=z_{Fe_2}$.

[c] esd's include uncertainties on neutron wavelength.

[d] For definitions see Ref. 34.

[e] The numbers in parentheses are esd's referred to the least significant digit. Scattering amplitudes for Ba, Y, Cu, Fe, and O taken as 0.525, 0.775, 0.7717, 0.954, and 0.5805×10^{-12} cm, respectively (Ref. 35).

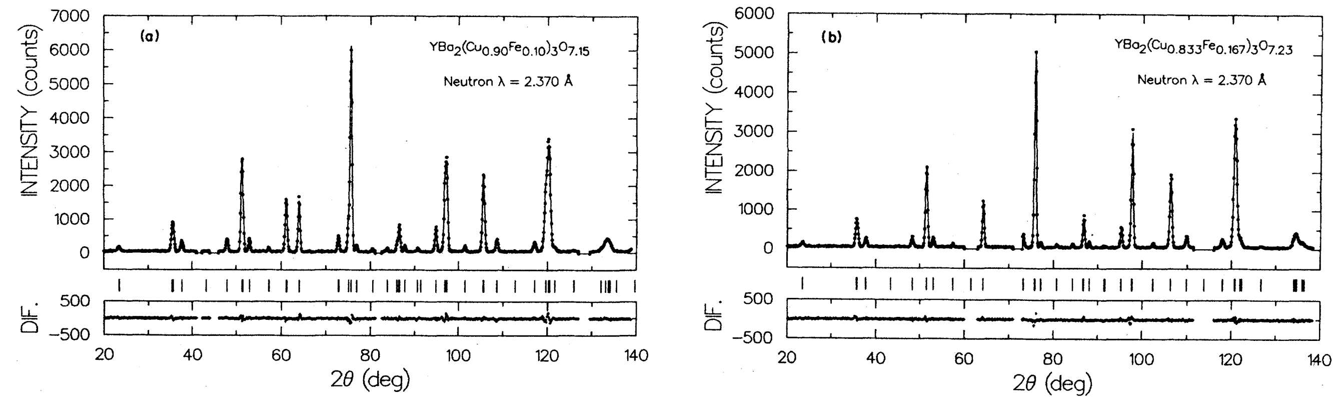

FIG. 3. Neutron-powder-diffraction pattern and the difference between the measured and the calculated intensities using the Rietveld profile refinement for (a) $YBa_2(Cu_{0.9}Fe_{0.1})_3O_{7.15}$ and (b) $YBa_2(Cu_{0.833}Fe_{0.167})_3O_{7.23}$.

tained using a statistical distribution of O(3) in a less symmetric site $(x, \frac{1}{2}, 0)$ and by refining a preferred orientation parameter. The fits for $x=0.10$ and 0.167 are shown in Figs. 3(a) and 3(b). The resulting structure models for both samples are listed in Table II.

The structure refinements confirm the picture that iron goes mainly onto Cu(1) sites. However, in part because of the similarity of the scattering factors of Cu and Fe, the present data cannot exclude the possibility that some of Fe substitutes onto Cu(2). The total oxygen contents for these specimens were determined in the refinement to be about 7.15 $(\delta=-0.15)$ for $x=0.10$ and 7.23 $(\delta=-0.23)$ for $x=0.167$. The lattice parameters determined in the profile refinement at room temperature for $x=0.10$ agree with those determined by x-ray diffraction, within the range of estimated standard deviations (esd). Also, the neutron data of the $x=0.167$ sample were analyzed for the presence of peaks originating from long-range antiferromagnetic ordering. No evidence for such peaks was found. Upper limits of integrated intensities for peaks with indexing of $(\frac{1}{2}, \frac{1}{2}, n/2)$ were at least one order of magnitude smaller than what would be expected for the type of magnetic ordering found in $YBa_2Cu_3O_6$ (Ref. 36) or $YBa_2Cu_2CoO_7$.[33]

C. Superconducting transition temperature

Superconducting transition temperature T_c measured by mutual inductance for the Fe substituted specimens are shown in Fig. 4. The filled circles are the midpoints of the transition and the vertical bars represent 10–90% of the whole transition. The width of the transition increases as the Fe content increases. The values of T_c of our specimens are higher than those observed by some others for the same Fe contents. For example, for $x=0.033$, Tarascon *et al.*[10] report T_c between 70–55 K, while for our $x=0.03$ specimen, T_c is between 85–80 K. The discrepancy may in part be caused by a difference in oxygen content, which depends on the detailed specimen preparation process.

The T_c versus Fe content curve has a negative curvature, a behavior reminiscent of T_c versus concentration of paramagnetic impurities.[37] dc magnetic-susceptibility measurements[38] show that the temperature dependence of normal state χ of the Fe-doped samples follows Curie-Weiss law. These results suggest that the Fe atoms form localized magnetic moments.

D. Electrical resistivity

The electrical resistivities as a function of temperature for six specimens, $0 \leq x \leq 0.05$, are shown in Fig. 5. All the samples up to $x=0.075$ show metallic behavior but, for $x=0.10$ between $T=150$ K and the onset of superconductivity, resistance rises as temperature is reduced. In agreement with the ac susceptibility measurements, the resistively measured superconducting transition width increases as Fe content increases. For $YBa_2Cu_3O_7$, the resistive transition width is only about 0.2 K, while for an Fe-containing sample with $x=0.05$, the transition width is about 7 K. It was also noted that the zero-resistance temperatures in Fig. 5 for all Fe contents are very near the onset (10% value) of the ac susceptibility transition for the same x (see Fig. 4).

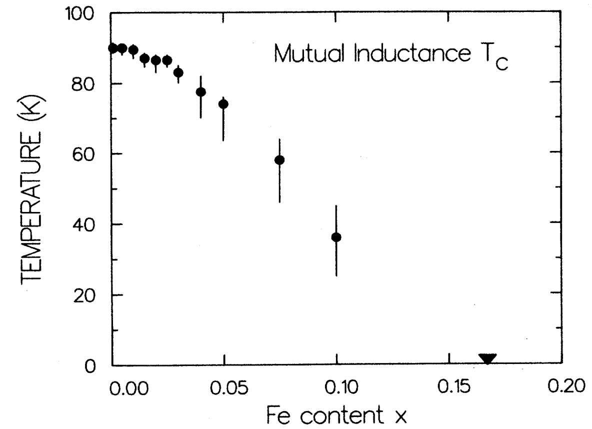

FIG. 4. Critical temperatures of $YBa_2(Cu_{1-x}Fe_x)_3O_{7-\delta}$ as the Fe concentration x.

The resistivities of the samples at room temperature and 100 K are plotted versus Fe content in Fig. 6. The resistivity values increase almost linearly with x. The resistivity ratio $\rho(300\ K)/\rho(100\ K)$ is about 3 for $x=0$ sample and about 2 for $x=0.05$. The systematic nature of variations in resistivity values and of temperature dependence of resistivity suggest that the specimens have been prepared in a consistent and reproducible manner.

E. Transmission electron microscopy and microstructures

The results of transmission electron microscopy performed on the specimens of $YBa_2(Cu_{1-x}Fe_x)_3O_{7-\delta}$ for compositions of $0 \leq x \leq 0.15$ are shown in Figs. 7–16.

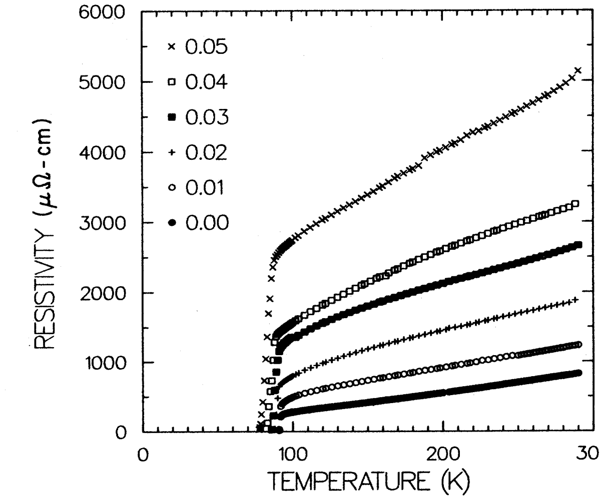

FIG. 5. Resistivity of $YBa_2(Cu_{1-x}Fe_x)_3O_{7-\delta}$ as a function of temperature for $0 \leq x \leq 0.05$.

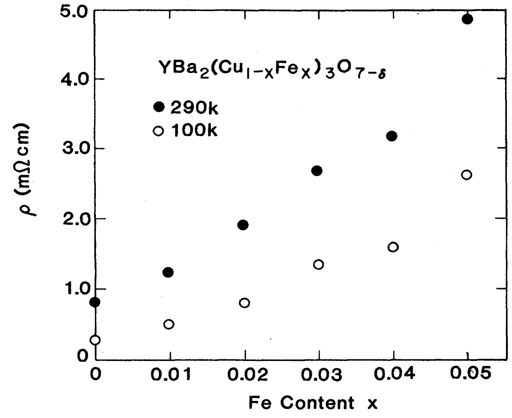

FIG. 6. Resistivity of $YBa_2(Cu_{1-x}Fe_x)_3O_{7-\delta}$ at 100 and 296 K as a function of the Fe concentration x.

They illustrate that the primary microstructural changes due to the substitution of Fe for Cu are (a) a systematic variation in the spacing between the twin boundaries and the eventual disappearance of twins and (b) the appearance and the disappearance of a tweed morphology and the associated diffuse streaks along the ⟨110⟩ directions in electron-diffraction (ED) patterns. These observed changes are separately discussed in detail for six composition ranges: (1) $x=0$, (2) $x=0.005$–0.015, (3) $x=0.02$, (4) $x=0.025$, (5) $x=0.03$–0.05, and (6) $x=0.10$–0.15. Then, in the discussion section, the interpretation of the images and the ED patterns, which vary with Fe, are discussed in terms of possible causes of these changes and their effects on superconducting properties of these specimens.

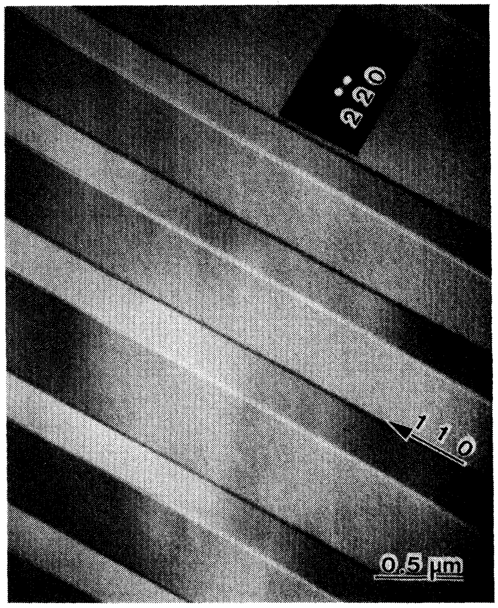

FIG. 7. A dark-field transmission electron micrograph of a $YBa_2Cu_3O_7$ taken with $g=\langle 110\rangle$ showing very large twins. The inset indicates the degree of the split at the ⟨220⟩ reflection due to the twin formation. In this case g is parallel to the twin boundary and the direction of the split is perpendicular to the boundary and g.

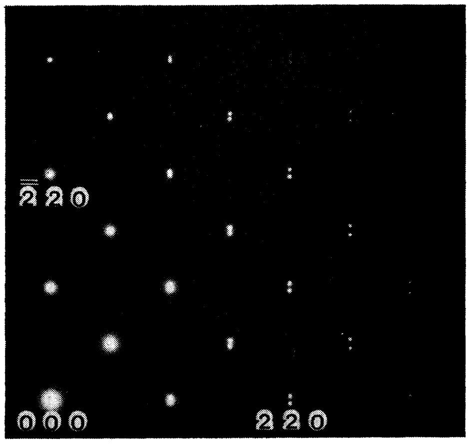

FIG. 8. A selected area electron-diffraction pattern from the area shown in Fig. 6. Note that the twin boundary is parallel to the $[hh0]$ direction and the split at the diffraction spots is zero at the $[\bar{h}h0]$ and maximum at the $[hh0]$.

1. $YBa_2Cu_3O_7$: $x=0$

Figure 7 displays a typical set of the (110)-type twins. These are formed as the result of the structural transformation (a tetragonal-to-orthorhombic phase) in $YBa_2Cu_3O_7$ during cooling from high temperature (~970 °C).[39] A corresponding ED pattern with the zone axis along the [001] direction is also shown in Fig. 8 with clearly separated $(hk0)$ spots, indicating that these spots are from the twins and the boundaries are along the (110)

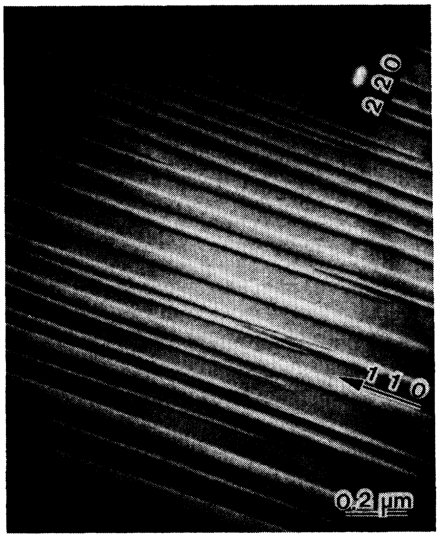

FIG. 9. A dark-field transmission electron micrograph of $YBa_2(Cu_{0.985}Fe_{0.015})_3O_{7-\delta}$ taken with $g=\langle 110\rangle$. Note that the size of the twins and the separation of the ⟨220⟩ spots are significantly reduced.

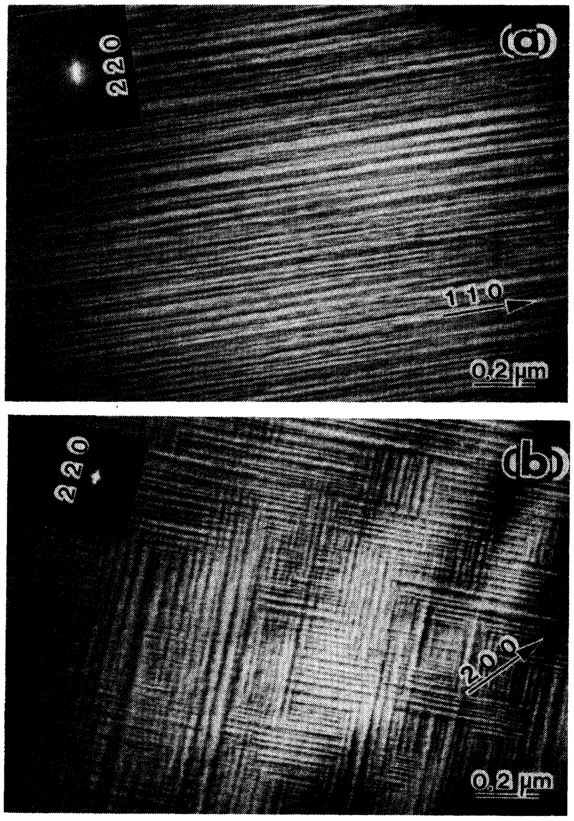

FIG. 10. Dark-field transmission electron micrographs of $YBa_2(Cu_{0.98}Fe_{0.02})_3O_{7-\delta}$ showing very finely divided twins from two different areas using $g = \langle 200\rangle$ to image the twins in both directions. The insets show appearance of very weak diffuse scattering streaks along the $\langle hh0\rangle$ and $\langle \bar{h}h0\rangle$ directions.

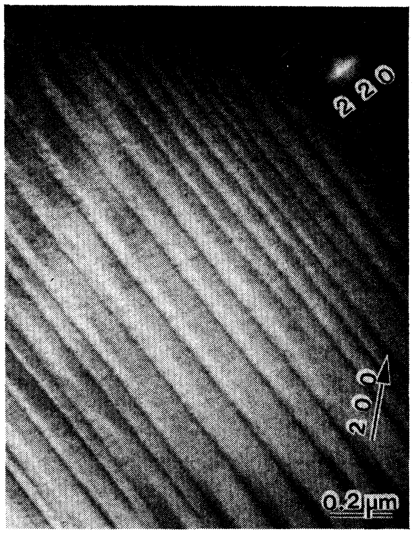

FIG. 11. A dark-field transmission electron micrograph of $YBa_2(Cu_{0.975}Fe_{0.025})_3O_{7-\delta}$ showing the twins and the tweed structure which are superimposed. The diffraction condition was $\langle 200\rangle$ to show the tweed in both of the $\langle hh0\rangle$ directions. The inset shows the reduced separation of the $\langle 220\rangle$ split and the increased intensity on the diffuse scattering streak.

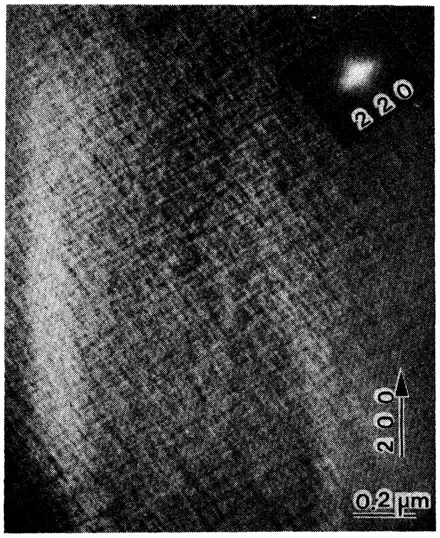

FIG. 12. A dark-field transmission electron micrograph of $YBa_2(Cu_{0.97}Fe_{0.03})_3O_{7-\delta}$ showing the tweedlike structure using $g = \langle 200\rangle$. Note that the $\langle 220\rangle$ reflection is not split and the diffuse scattering is stronger than that for $x \lesssim 0.025$.

planes. Shown with the dark-field image of the twins (Fig. 7) are the (220) diffraction spots, illustrating the orientation of the split between the two diffraction spots due to the matrix and the twins. In this case, the twin boundaries are parallel to the [110] direction and the split is in the $[\bar{1}10]$ direction. In the specimens of pure $YBa_2Cu_3O_7$, the typical spacing between the twin boundaries was > 200 nm and is larger than normally reported values (~ 100 nm).

Also, in the area where the twin-boundary spacing is $\lesssim 100$ nm, very sharp streaks at the zero- and low-order diffraction spots are observed. These streaks are in the direction perpendicular to the twin boundaries and are due to very thin layers of a nonorthorhombic material at

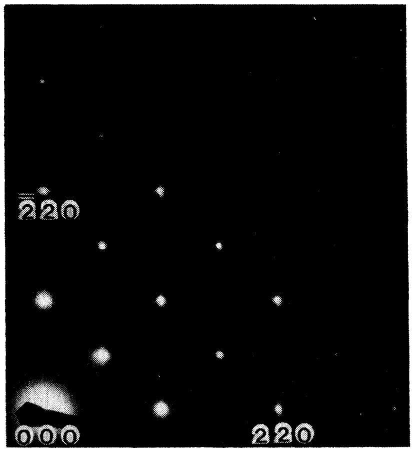

FIG. 13. A $\langle 001\rangle$ zone selected area electron-diffraction pattern form the area in Fig. 12 showing the crossed diffuse scattering at all $\langle hk0\rangle$ diffraction.

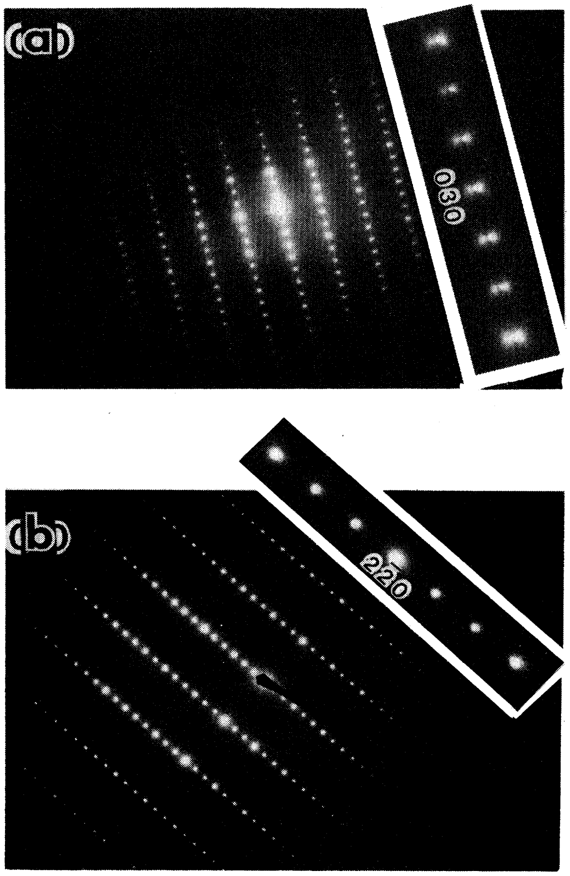

FIG. 14. Selected area electron-diffraction patterns from (a) the ⟨100⟩ and (b) the ⟨110⟩ zones of $YBa_2(Cu_{0.97}Fe_{0.03})_3O_{7-\delta}$. The insets show (a) the presence of and (b) the absence of the diffuse scattering in the ⟨100⟩ and the ⟨110⟩ zones, respectively.

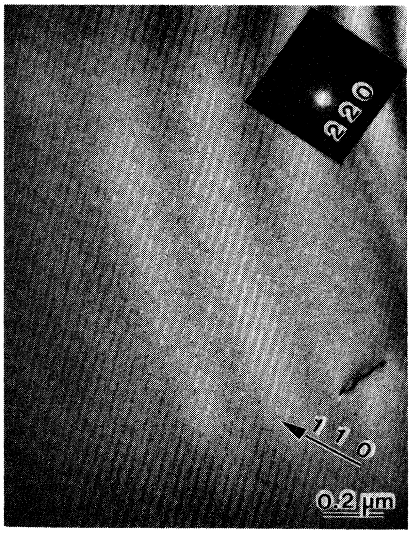

FIG. 15. A dark-field transmission electron micrograph from $YBa_2(Cu_{0.90}Fe_{0.10})_3O_{7-\delta}$. At this composition, the tweedlike structure is not clearly visible but weak diffuse streaks exist (see inset) $g=\langle 200\rangle$.

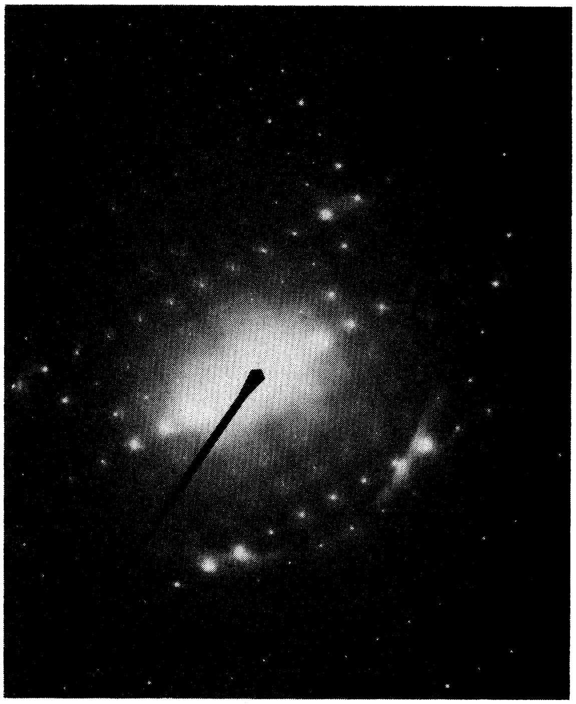

FIG. 16. A selected area diffraction from $YBa_2(Cu_{0.85}Fe_{0.15})_3O_{7-\delta}$ showing the appearance of diffuse scattering which is centered at a position along the ⟨*hh*0⟩ direction and at $0.167(\sqrt{2}/a)$. The electron-diffraction pattern is taken by tilting ~15° away from the ⟨001⟩ zone along the [*hh*0] direction.

the twin boundaries.[40] From the length of the streak, the thickness of the twin-boundary layer is estimated to be 1.0–1.5 nm. These streaks are very weak and are not well reproduced in glossy photographs.

2. $YBa_2(Cu_{1-x}Fe_x)_3O_{7-\delta}$: $0.005 \leq x \leq 0.015$

In this composition range, the following subtle changes, which are more obvious in the specimens with higher Fe contents, begin to appear in the ED patterns and in the images.

(a) A second set of weak diffuse streaks along the [110] directions, which form a cross pattern, also appears at $x=0.015$ as shown in the inset of Fig. 9. (Unfortunately, these diffuse streaks do not reproduce.) These are easier to observe at higher-order diffraction spots. Associated with the above streaks are very fine (<5 nm) elongated features between the boundaries. Both of these are thought to be an early stage of formation of the tweed structure, which will be discussed in detail for $0.03 \leq x \leq 0.05$.

(b) The separation between the split twin-diffraction spots decreases with increasing Fe content, as expected from the lattice parameter measurements by x-ray diffraction (see Fig. 2).

(c) Also, as shown in Fig. 9, the spacing between the twin boundaries of these Fe-substituted specimens decreases significantly from those for the pure oxide in Fig. 7. Furthermore, many narrow twins terminate in the matrix rather than at the grain boundaries or at the intersecting twins. These terminating twins are rare in "well-prepared" specimens of pure $YBa_2Cu_3O_{7-\delta}$ such as the one in Fig. 7.

(d) Finally, the sharp streaks at the low-order diffraction spots become shorter and less sharp than those in the pure specimen. The shorter streaks indicate that the twin-boundary layers are thicker (i.e., 1.3–2.0 nm) than those for the pure specimen, while the lack of definition suggests that the interface between the matrix and the boundary layers is not as sharp as for the pure case.

3. $YBa_2(Cu_{1-x}Fe_x)_3O_{7-\delta}$: $x=0.02$

At this composition, a drastic change in microstructure is apparent in Figs. 10(a) and 10(b). The typical spacing between the twin boundaries is ~20 nm in contrast to several tens of nm or greater for the specimens with concentrations of Fe below $x<0.02$. Also shown in Fig. 10(b) are very fine crossing twins, which appear in a considerable number of the grains. In these TEM specimens, approximately 80 out of 100 grains observed contain these fine twins. However, the remaining portion of the grains exhibit relatively larger twins which are similar to those shown in Fig. 9. Occasionally, there are areas with small (10–20 nm) twins which are widely dispersed in the matrix. Most of these twins terminate in the matrix. In order to check the possibility that a variation in Fe concentration might be associated with the large differences in the twin-boundary spacing, chemical analysis of these areas was performed in the microscope using an energy dispersive x-ray detector. No detectable difference in the Fe content was measured among these areas. However, considering the limited sensitivity of this type of analysis, it is still possible to have small local variations in the compositions which might cause variations in the spacings.

Compared with specimens having lower Fe contents, the intensity of the diffuse streaks along ⟨110⟩ directions at diffraction spots is greater and the distance between the two split spots is smaller (see Fig. 10 inset). These diffuse streaks form a clear cross pattern. In some areas the presence of a very fine tweedlike structure is evident between the widely spaced twin boundaries. However, at this composition, the image contrast from the tweedlike structure is still weak and difficult to show in reproduction of the images. The diffuse streaks and the tweedlike structure will be further discussed for specimens with higher Fe contents. The very sharp streaks at the central region of the ED pattern became stronger than those for $x\leq 0.015$ due to the high density of the twins. However, their length is further decreased, indicating the boundary-layer thickness is approximately 1.6–2.4 nm.

4. $YBa_2(Cu_{1-x}Fe_x)_3O_{7-\delta}$: $x=0.025$

At $x=0.025$, a large fraction of the specimens contain twins of relatively large spacings (see Fig. 11), similar in size to specimens with $x=0.015$, while very fine twins such as seen for $x=0.02$ are also found in the remaining areas. Also, the diffuse streaks in the ⟨110⟩ directions as well as the tweedlike structure which coexists with the twins are prominent in Fig. 11. Furthermore, the split twin diffraction spots have nearly converged to one spot as shown in the inset in Fig. 11 and the sharp streaks at the low-order diffraction spots are no longer observed indicating that the distinction between the boundary layer and the matrix became insignificant.

5. $YBa_2(Cu_{1-x}Fe_x)_3O_{7-\delta}$: $0.03\leq x\leq 0.05$

In this composition range, the twins are absent in the transmission electron micrograph image, except occasionally in small regions. The tweedlike structure is the only microstructural feature observed in transmission electron microscopy. This is illustrated in Fig. 12, where a grain was oriented such that the electron beam was approximately parallel to the ⟨001⟩ direction. From the image in Fig. 12, the tweedlike structure appears to consist of mutually perpendicular platelets which are ~100 nm long and ~5 nm wide in the a-b plane. Associated with this structure are, as before, the diffuse streaks along both of the ⟨110⟩ directions at each of the diffracted spots as shown in the ED pattern of a specimen with $x=0.03$ (Fig. 12). (While the diffuse streak is weak and not easily reproduced in prints, it is clearly illustrated in the inset in Fig. 12 for the ⟨220⟩ spot.) In order to further study the nature of these streaks, the diffraction patterns in two other zones (⟨100⟩ and ⟨110⟩) are illustrated in Fig. 13 (*a* and *b*, respectively). In the enlarged ⟨03l⟩ diffraction spots, as shown in the inset in Fig. 14, weak diffuse scattering extends toward the ⟨0k0⟩ directions and the width of the scattering along ⟨001⟩ directions is less than $\sim\frac{1}{5}$ of the distance between the ⟨00l⟩ and ⟨00$l+1$⟩. The latter indicates that the individual small platelike region of the tweedlike structure extends approximately 10–20 nm along the c direction. This observation is contrary to the result of Bordet *et al.*[41] in which the streak extended significantly in the ⟨001⟩ direction, implying that the tweed structure is not coherent in the ⟨001⟩ direction. (This is also different from the oxygen-vacancy ordering in the CuO planes in oxygen-deficient $YBa_2Cu_3O_{7-\delta}$, where the ordering is not coherent from one CuO plane to another along the c axis. In that case the streaks due to the ordered plane extend along the ⟨001⟩ direction.[42]) The diffraction pattern along the ⟨110⟩ zone [Fig. 14(b)] does not show diffuse scattering along the ⟨hh0⟩ directions and only weak scattering along the ⟨001⟩ directions. From this we conclude that one of the streaks at the (hh0)-type spots in the ⟨001⟩ zone diffraction pattern in Fig. 13 is likely to be due to double scattering (e.g., at the ⟨hh0⟩ spots the streak along the [110] direction is due to double scattering and the streak along the [$\bar{1}$10] is real and due to the plateletlike regions which are parallel to the [110] direction). Another important feature is that the length of the streak increases as the order of the diffraction spot increases in the reciprocal space away from the central beam. (Since the intensity of the diffused streaks are so weak, this effect is not observable in Fig. 13 but is easily seen in the negatives of the ED patterns.) The above results indicate that these streaks are not simply due to the small size of the platelets but also to an additional source, such as a variation in Δa or strain at the boundary as will be discussed later.

6. $YBa_2(Cu_{1-x}Fe_x)_3O_{7-\delta}$: $x=0.10-0.15$

For Fe contents $x=0.10$ and 0.15, there is no tweed structure in the image, at least at our magnification of 50–100 K but, some very fine microstructural features are visible. (See Fig. 15). However, the diffuse streaks, which were seen at lower compositions, are still observed (as shown in the inset of the figure), but they are significantly weaker than those in the specimens with $0.03 \leq x \leq 0.05$. Furthermore, for $x=0.15$, additional diffuse scattering is observed around the $\langle hk0\rangle$ diffracted beams between the $(00l)$ and $(00l+1)$ planes in the reciprocal space as shown in Fig. 16. This may be due to ordering of Fe or oxygen in the CuO planes. The details of this aspect of the work will be discussed elsewhere.[43]

IV. DISCUSSION

A. Electron microscopy

1. The twin-boundary layers

Very sharp streaks at the low-order diffraction spots in the ED patterns are observed for $x \leq 0.02$. The lengths of these streaks decrease with increasing contents of Fe. As stated earlier, from the lengths, the thickness of the nonorthorhombic layers are estimated to be 1.0–1.5 nm at $x=0$ and 1.6–2.4 nm at $x=0.02$. (However it is possible that the reduction in length of the streaks may be partly due to roughening of the interface between the matrix and the layer which is associated with the formation of the early stage of the tweedlike structure.)

Although, we have observed the twin-boundary layers in a number of other specimens, (e.g., Zn- and Ni-substituted 1:2:3) by the electron diffraction technique,[40] the existence of such layers has not been widely discussed previously.[44,45] This is surprising considering its significance in understanding the role of the twin boundaries in determining superconducting properties of $YBa_2Cu_3O_7$. Barry[45] reported possible observation of a "twin boundary phase " in *some* of the $YBa_2Cu_3O_7$ specimens. Using high-resolution electron microscopy, he observed regions approximately 3 monolayers thick (~0.8 nm), which were not orthorhombic, at the twin boundary. On the other hand, Sarikaya and co-workers[44] suggested that the twin boundary is nonorthorhombic and has a thickness of 3–5 nm as measured by a converging beam electron-diffraction technique. Our estimate for the layer thickness for the pure $YBa_2Cu_3O_7$ is in accordance with that of Barry. Furthermore, we believe that the twin boundaries in $YBa_2Cu_3O_7$ or similar specimens always contain thin layers which are different from the orthorhombic matrix. However, when the twin-boundary spacing is large, it is difficult to observe these layers due to the limited area contributing to the intensity of the streaks. The structural difference between the layer and the matrix may be so slight that it is not easily observed in the high-resolution microscopy.

2. Twin-boundary spacings

In order to discuss effects of the Fe substitution for Cu on the spacing between the twin boundaries, we will first consider the general factors which affect the spacing. According to an equation derived by Welch,[46] the twin-boundary spacing d depends on the grain size g, the orthorhombicity,

$$\phi \simeq (1-[a/b]) \simeq \Delta a_0 = 2(b-a)/(b+a)\,,$$

the interface energy of the twin boundary γ and the elastic shear modulus M as

$$d \simeq (g\gamma/cM\phi^2)^{1/2}\,, \tag{1}$$

where c is a constant of the order of the unity and g is measured *along the twin boundary in the* $\langle 110\rangle$ *direction*. Note that this expression is similar to that obtained by Arlt and Sasko[47] but their value of the constant c is $1/128\pi$. Sarikaya and co-workers[44] have also derived a slightly different expression for d, which does not contain the grain size dependence. Recent experimental results[48,49] have shown that dependence of d on the grain size is indeed $\sim\sqrt{g}$. Furthermore, a careful measurement of d and g along the $\langle 110\rangle$ direction indicated that the constant c is approximately one rather than $1/128\pi$.[50]

Although the size of the grains decreases with increasing Fe content, this decrease cannot alone explain the reduction in the twin spacing which was observed in this study. The grain size at $x=0.02$ compared to that at $x=0$ is reduced by about a factor of 4. This reduction in the grain size predicts only a factor of two smaller twin boundary spacings. This predicted variation is in fact much smaller than that observed. Thus, we will neglect this factor for the present discussion.

The orthorhombicity ϕ (or Δa_0) (as measured by x-ray diffraction) diminishes with increasing Fe content x. Since d is inversely proportional to the orthorhombicity Δa_0, our expression predicts the spacing to increase with the increasing Fe content. However, the twin-boundary spacings actually decreases with the addition of Fe up to $x=0.02$, as shown in Figs. 7–10. At $x=0.025$, approximately one-half of the specimens contain relatively large twins, the other half fine twins. Finally, the twins disappear for $x \geq 0.03$. This variation in the spacing indicates that the substitution of Fe for Cu lowers the value of the twin-boundary surface energy γ, favoring a larger number of the twins for $x \leq 0.02$ than for the pure 1:2:3. (This is also suggested by Shaw *et al.*[48] based on the expression by Arlt and Sasko.[47]) At $x=0.025$ the situation becomes less clear. However, it is reasonable to suggest that at this composition, the effects of decreasing values of γ and $(\Delta a_0)^2$ are comparable in determining the values of d, and small local variation in the Fe and/or O content may cause the local differences in d which were observed (i.e., ~50% very fine and ~50% medium-size twins). Thus, the variations in the spacing d are basically due to the lowering of the interfacial energy γ by Fe additions. Unfortunately, it is very difficult to estimate the value of γ in this system and at present it is not clear how such small substitutions of Fe can influence γ so strongly, e.g., $\gamma(x=0)/\gamma(x=0.02)\simeq 10^2$ since $d(x=0)\simeq 200$ nm and $d(x=0.02)\simeq 20$ nm. However, the above result is not unreasonable in light of the fact that replacement of Fe in the CuO chain has a strong effect on determining the location of O in the CuO planes and has increased the thickness of the twin-boundary layers and thus reduced the strain energy of the boundary in comparison to those for the pure oxide.

The variations in the twin-boundary spacing due to the substitution of Fe for Cu are qualitatively described by assuming a greater reduction in γ with Fe than in $(\Delta a_0)^2$ in Eq. (1). However, the tweed structure coexists with the twins for $0.015\leq x\leq 0.025$. As described below, the tweed structure is thought to consist of fine ($\lesssim 5$ nm) orthorhombic domains related by the twinlike boundaries. (See Sec. IV A 3). It is not clear why formation of these twinlike domains does not release the strain energy due to the transformation from the tetragonal-to-orthorhombic phase to avoid formation of the twins. It appears from the above result that the twins are primarily determined by the average Δa_0 (such as measured by x-ray-diffraction techniques) rather than the local Δa of the scale of <5 nm in the domains.

3. The "tweed" structure and the diffuse streaks

Formation of the tweed morphology is quite common in the 1:2:3 system where the substitution of other elements such as Ga[28], Al[29], and Co[30] causes the crystallographic structural changes from the orthorhombic-to-tetragonal phase at sufficient levels of the substitution of Cu by each of these elements (e.g., $x\sim 0.03$). A similar tweed structure, somewhat coarser than the present one and an associated diffuse scattering, can also be observed in oxygen deficient $YBa_2Cu_3O_{7-\delta}$.[30,51,52] There have been some attempts to interpret the diffuse scattering and the tweedlike morphology in these systems.[30,40,53,54]

The first observation of the diffuse streaks and the tweedlike structure was reported by Iijima *et al.*[52] in $YBa_2Cu_3O_{7-\delta}$ by heating the specimens in an electron microscope. The size of the tweedlike structure was significantly greater than those observed in the present study of alloyed $YBa_2Cu_3O_7$. Independently, a similar observation was also made by van Tendeloo and Amelinckx[55] by the same technique. The latter attributed the streaks to very fine twins without specifying the size while Iijima *et al.*[52] suggested that these are from the small twin*like* structure ($\sim$16 nm). In a later article, Ichihashi *et al.*[30] proposed that this structure is formed by having small elongated islands of the tetragonal phase in the orthorhombic phase. The islands are separated from the orthorhombic matrix by thin transition layers. More recently, based on high-resolution electron microscopy, Roth *et al.*[54] and Sastry, Wördenweber, and Freyhardt[56] suggested without detailed explanations that the diffuse streaks in $YBa_2(Cu_{0.95}Fe_{0.05})_3O_{7-\delta}$ are due to very small 2–5 nm orthorhombic domains. [Although Sastry *et al.* claimed that they have measured $a=0.383$ and $b=0.39$ nm for a Fe-substituted specimen from a high-resolution electron micrograph, this is unlikely. In order to measure Δa of $\sim$1%, it is required to measure distances for 50–100 lattice planes in the two directions, i.e., a and b. Since the domain is $\sim$5 nm, each domain can contain only 10–15 ($\simeq$5/0.38) lattice planes in the a or b direction. Thus, it makes it nearly impossible to measure a and b to the accuracy of 1%.]

On the other hand, Bordet *et al.*[41] proposed that the streaks are due to closely spaced linear clusters of Fe cation chains extending along the $\langle 110\rangle$ directions and separating the orthorhombic domains. In addition, a study of $YBa_2(Cu_{1-x}Fe_x)_3O_{7-\delta}$ by high-resolution electron microscopy led Hiroi *et al.*[53] to conclude that the streaks and the tweedlike structures for $x=0.04$ are due to microdomains of the orthorhombic phase. They furthermore suggested that the domains are squares and each corner of the square domain is occupied by Fe atoms. However, it seems likely that the position of the Fe atoms in the lattice determined at temperatures well above the tetragonal-to-orthorhombic phase transformation ($>700\,^\circ$C). Thus, it is difficult to imagine any interaction forces capable of ordering a small number of Fe atoms in the ways described. Although the above suggestions (the microdomains of the orthorhombic phase and the fine embryos of the tetragonal phase in the orthorhombic phase), appears to be appropriate in describing the tweedlike structure and the associated diffuse streaks in some cases, we find neither one of them is sufficient or detailed enough to satisfactorily explain the evolution of the microstructures and the ED patterns in the $YBa_2(Cu_{1-x}Fe_x)_3O_{7-\delta}$ with $0.05\leq x\leq 0.15$.

In order to discuss possible microstructural origins of the tweedlike structure and the streaks in the ED patterns of $YBa_2(Cu_{1-x}Fe_x)_3O_{7-\delta}$ specimens, it is important to note the following: Common to the electron diffraction observations for $0.03\leq x\leq 0.15$ are narrow streaks of diffuse scattering along the [110] (and the $[1\bar{1}0]$) direction through most of the reflections, thus forming a cross. Exceptions are the $[hhl]$ (and the $[h\bar{h}l]$) reflections where there is a diffuse streak in only one direction, namely, the $[1\bar{1}0]$ and [110] direction, respectively. Another exception occurs at the $(00l)$ reflections where there appear to be no diffuse streaks. The above is also true for the diffuse streak portion of the ED patterns for $x\simeq 0.015$–0.025 but is not as clear as in the cases for $x\gtrsim 0.03$.

A distribution of diffuse scattering similar to that described above is expected for twin related domains when the $(1\bar{1}0)$ and the equivalent (110) planes are the twin planes for a continuous range of b/a ratios ranging from 1.0 to $b/a=3.88/3.82=1.016$ (i.e., the b/a ratio of $YBa_2Cu_3O_7$) within the illuminated area. This would apply even if the domains were large, provided the electron beam had a sufficient diameter to probe statistically all b/a ratios. In that case, the majority would be tetragonal.

Very thin coherent domains which are twin related will also give similar streaks of diffuse scattering due to their limited thickness (shape effect) even for the unlikely situation that $a=b$ [if, e.g., the chains of oxygen atoms are rotated 90° across the (110) twin boundary].

An observable difference between these two extreme cases is that for larger microtwins with $b/a \neq 1$ the length of the diffuse streaks will increase with increasing distance from the (001) axis in reciprocal space observed for $0.015 \leq x \leq 0.05$. For the other extreme where $a = b$, the length of the streaks would be the same for all reflections (as seen for $x = 0.10$ and 0.15). Due to multiple scattering, which tends to redistribute the diffuse scattering among the reflections, it can be difficult to distinguish between these two cases. There is, however, evidence that at lower Fe content ($x \leq 0.05$) $b/a > 1$, whereas for $x = 0.10$ and $x = 0.15$ the shape effect dominates and masks any possible effect of $b/a > 1$. Also, it is expected that the first case would result in a stronger contrast than the second in the images as shown in Figs. 12 and 15, respectively. Furthermore, the first description is very similar to that proposed by Ichihashi *et al.*[30] if one interprets their transition layers and tetragonal islands as the regions where Δa semiperiodically varies along the [110] directions. In this composition region, the contrast in the image and the streaks is also possibly due to the strain along the [110] direction.[57]

From these observations one cannot deduce the exact structure of the domains. As suggested by others, the observations do strongly suggest that we are dealing with microtwins in the (110) planes, possibly with a b/a ratio less than for pure $YBa_2Cu_3O_7$ but larger than 1. The thickness of the microtwins decreases from ~4.0 to ~1.5 nm when the Fe content increases from 3% to 15%. For $x = 0.15$ we also observe a tendency towards periodic twins with a period of $3.87 \times 6\sqrt{2} = 1.63$ nm. This observation will be discussed in more detail elsewhere.[43]

B. Superconducting properties

The possibility of enhanced values of T_c at the twin boundary has been suggested in Refs. 6 and 7. Increased values of T_c in $YBa_2Cu_3O_7$ near grain boundaries is predicted to become observable when the twin-boundary spacing is on the order of ~20 nm or smaller. However, in spite of the fact that the spacing is reduced to 10–20 nm for specimens with Fe $x = 0.02$, T_c continues to decrease smoothly with increasing Fe content. This suggests that the existence of such high-T_c regions at the twin boundary is unlikely, although it can be argued that the addition of Fe has changed the nature of the boundary such that the condition leading to higher T_c at the boundary is destroyed. In fact, the boundary layer is nonorthorhombic and is expected to have a reduced superconductivity as suggested by Deutscher and Müller.[9]

In trying to determine various aspects of crystallographic and/or structural properties which may be important for achieving high critical temperatures in these oxides, the possible importance of the bond length [Cu(1)−O(1)] between the Cu in the chain and the oxygen just above (sometimes called "sticks") was pointed out based on studies of oxygen-deficient[58] Co-doped $YBa_2Cu_3O_{7-\delta}$.[59] However, if the lattice parameter c along the ⟨001⟩ directions is taken as an indication of the change in the length of the "stick," the variation in the length, which is associated with the Fe substitutions, is negligible since the value of c decreased only by ~0.14% from $x = 0$ to 0.15. [In pure $YBa_2Cu_3O_{7-\delta}$, the increase (~1.3%) in c is accompanied by a decrease (~1.67%) in the "stick" length for the variation in oxygen of $\delta = 0$ to $\delta \simeq 0.8$. Thus, the above assumption in regard to the relationship between the changes in c and the "stick" length is likely to be appropriate.] Thus, in contrast to the Co substituted $YBa_2Cu_3O_7$,[59] the value of T_c in this system diminished to zero at $x \simeq 0.15$ in spite of the very small change in the apparent "stick" length.

While there are a limited number of direct measurements of the [Cu(1)−O(1)] bond length by neutron and x-ray diffraction for $x \leq 0.167$ (Refs. 24, 41, and 54) in the $YBa_2(Cu_{1-x}Fe_x)_3O_{7-\delta}$ system, the values reported by these studies are not consistent enough to draw a definite conclusion on the relationship between the bond length and the values of T_c. For example, our neutron-diffraction data show that the lengths of 0.1853, 0.1840, and 0.1849 nm for $x = 0$, $x = 0.10$, and 0.167, respectively. (The length for $x = 0.167$ was adjusted for the room-temperature value using the data of Roth *et al.*[54] at 3 and 300 K for $x = 0.05$.) Roth *et al.*[54] reports that the length is 0.1829 and 0.1855 nm for $x = 0.05$ measured by neutron and x-ray diffraction, respectively, while Bordet *et al.*[41] measured the length to be 0.1838 nm for $x = 0.07$ by neutron diffraction. Furthermore, Roth *et al.*[54] believe that their single-crystal x-ray-diffraction result is more precise than their neutron data on the length. Also, Tao *et al.*[24] report the length of the Cu(1)−O(1) bond to be 0.1791 nm in their $YBa_2Cu_{2.5}Fe_{0.5}O_{7-\delta}$ (this is equivalent to $x = 0.167$). However, the value of the "c" parameter for this specimen is 1.1637 nm which is substantially greater than our values for c for the same composition. It is likely that the amount of oxygen in their specimen is less than the maximum which the composition can absorb. Thus, in the Fe-substituted $YBa_2Cu_3O_{7-\delta}$, a clear dependence of T_c on the "stick" length could not be established from the neutron- and x-ray-diffraction data in contrast to the result which was reported by Miceli *et al.*[59] on the Co-substituted $YBa_2Cu_3O_{7-\delta}$. This could be due to the fact that such a relationship does not apply at least for the Fe-substituted system and/or the precision in the determinations of the length is not high enough, particularly when it is measured on different specimens by different groups of researchers.

A measurement of the carrier concentration n as determined by the Hall coefficient[60] indicates a smooth decrease of n as the Fe concentration is increased, in the same manner as for oxygen deficient $YBa_2Cu_3O_{7-\delta}$. This result supports the importance of large n for achieving high-T_c values[61] and suggests that the increasing values of resistivity with x of $YBa_2(Cu_{1-x}Fe_x)_3O_{7-\delta}$ are associated with reduced carrier density. Furthermore, measurements of electronic specific-heat coefficient for the similar Fe-substituted specimens[62] show decreasing strength of specific-heat jumps at T_c with increasing Fe. This may also be due to the decrease of n. However, it is not clear how the Fe atoms in the CuO plane influence the CuO_2 plane without significant changes in the length of the "stick," since the CuO_2 plane is generally accepted as the region of the crystal where the essential part of superconductivity is taking place in these high-T_c layered oxides.

The most interesting aspects of the influence of microstructural variations due to the Fe substitution are its effect on intragrain critical current densities and critical magnetic fields. Due to the fact that the only obvious defects in $YBa_2Cu_3O_7$ are the twin boundaries and that critical current densities of single-crystal or oriented films and bulk single crystals are very high in the *a-b* plane, the twin boundaries are thought to be strong pinning sites.[8,63,64] If this is the case, the value of J_c for a specimen with $x = 0.02$ Fe should be significantly higher than that for the pure $YBa_2Cu_3O_7$. Furthermore, the fine tweedlike structure observed for the specimens with $0.03 \leq x \leq 0.05$ may also be expected to act as effective pinning sites for the flux lines. However, disappointingly and as also found by other,[65,66] preliminary measurements of magnetization on *c*-oriented powders of these specimens indicate that the intragrain J_c decreases with increasing Fe in spite of microstructural changes which appear to be favorable for flux pinning.[67] The details of this result as well as the effects of other elemental substitutions such as Ni, Cr, Zn, Al, and Ga on the intragrain current densities will be discussed elsewhere. However, some preliminary suggestions can be made. (1) Either the twin-boundary planes are not effective pinning sites, or the substitution of Fe for Cu in the CuO plane modifies the structure of the twin-boundary region (e.g., widen the boundary thickness) such that the pinning strength of the boundary is reduced. (The spatial modulation of the electronic properties, which is pertinent for pinning, becomes too gradual for flux pinning in the tweedlike structure.) (2) The reduction in the carrier density may also influence the values of the intragrain critical current densities in the Fe-substituted 1:2:3 oxides. Finally, (3) as described by Wödenweber *et al.*,[65] the reduction in the H_{C2} with the Fe substitution reduces the value of J_c.

ACKNOWLEDGMENTS

The authors are grateful for very helpful discussions with D. O. Welch. The authors are also grateful to Dr. M. Kitano for bringing their work on the Fe-substituted $YBa_2Cu_3O_7$ to the attention of one of the authors (M.S.) Peter Zolliker gratefully acknowledges financial support from the Swiss National Science Foundation. This work was performed under the auspices of the U.S. Department of Energy, Division of Materials Sciences, Office of Basic Energy Sciences under Contract No. DE-AC02-76CH00016.

---

*Present address: Department of Physics, University of Oslo, Blindern, Norway.

[1] M. K. Wu, J. R. Ashburn, C. J. Torng, P. H. Hor, R. L. Meng, L. Gao, Z. J. Huang, Y. Q. Wang, and C. W. Chu, Phys. Rev. Lett. **58**, 908 (1987).

[2] A. R. Moodenbaugh, M. Suenaga, T. Asano, R. N. Shelton, H. C. Ku, R. W. McCallum, and P. Klavins, Phys. Rev. Lett. **58**, 1885 (1987).

[3] P. H. Hor, R. L. Meng, Y. Q. Wang, L. Gao, Z. J. Huang, J. Bechtold, K. Forster, and C. W. Chu, Phys. Rev. Lett. **58**, 1891 (1987).

[4] J. M. Tarascon, W. R. McKinnon, L. H. Greene, G. W. Hull, and E. N. Vogel, Phys. Rev. B **36**, 226 (1987).

[5] P. K. Gallagher, H. M. O'Boyan, S. A. Sunshine, and D. W. Murphy, Mater. Res. Bull. **22**, 995 (1987).

[6] M. M. Fang, V. G. Kogan, D. K. Finnemore, J. R. Clem, L. S. Chumbley, and D. E. Farrell, Phys. Rev. B **37**, 2334 (1988).

[7] F. M. Mueller, S. P. Chen, M. L. Prueitt, J. F. Smith, J. L. Smith, and D. Wohlleben, Phys. Rev. B **37**, 5837 (1988).

[8] P. Chaudhari, Jpn. J. Appl. Phys. **26-3**, 2023 (1987).

[9] G. Deutscher and K. A. Müller, Phys. Rev. Lett. **59**, 1745 (1987).

[10] J. M. Tarascon, P. Barboux, P. F. Miceli, L. H. Greene, G. W. Hull, M. Eibschutz, and S. A. Sunshine, Phys. Rev. B **37**, 7458 (1988).

[11] Y. Maeno, T. Tomita, M. Kyogku, S. Awaji, Y. Aoki, K. Hoshino, A. Minami, and T. Fujita, Nature (London) **328**, 512 (1987).

[12] Y. Maeno, M. Kato, Y. Aoki, and T. Fujita, Jpn. J. Appl. Phys. **26**, L1982 (1987).

[13] C. W. Kimball, J. L. Matykiewitz, J. Giapintzakis, H. Lee, B. D. Dunlap, M. Slaski, F. Y. Fradin, C. U. Segre, and J. D. Jorgensen, in *High Temperature Superconductors,* edited by M. B. Brodsky, R. C. Dynes, K. Kitazawa, and H. L. Teller, Materials Research Society Symposia Series, Vol. 99 (Materials Research Society, Pittsburgh, 1988) p. 107.

[14] S. B. Oseroff, D. C. Vier, J. F. Smyth, C. T. Salling, S. Schultz, Y. Dalichaouch, B. W. Lee, M. B. Maples, Z. Fisk, J. D. Thompson, J. L. Smith, and E. Zirngiebl, Solid State Commun. **64**, 241 (1987).

[15] Y. K. Tao, J. S. Swinnea, A. Manthiram, J. S. Kim, J. B. Goodenough, and H. Steinfink, J. Mater. Res. **3**, 248 (1988).

[16] T. J. Kistenmacher, W. A. Bryden, J. S. Morgan, K. Moorjani, Y.-W. Du, Z. Q. Qiu, H. Tang, and J. C. Walker, Phys. Rev. B **36**, 8877 (1987).

[17] Z. Q. Qiu, Y.-W. Du, H. Tang, J. C. Walker, W. A. Bryden, and K. Moojani, J. Magn. Magn. Mater. **69**, L221 (1987).

[18] C. Blue, K. Elgaid, I. Zitkowvsky, P. Boolchand, D. McDaniel, W. C. H. Joiner, J. Oostens, and W. Huff, Phys. Rev. B **37**, 5905 (1987).

[19] M. Mehbod, P. Wyder, R. Deltour, Ph. Duvigneaud, and G. Naessens, Phys. Rev. B **36**, 8819 (1987).

[20] E. R. Bauminger, M. Kowitt, I. Flener, and I. Nowik, Solid State Commun. **65**, 123 (1988).

[21] R. Gomez, S. Aburto, M. L. Marquina, M. Jimenez, V. Marquina, C. Quintanar, T. Akachi, R. Escudero, R. A. Barrio, and D. Rios-jara, Phys. Rev. B **36**, 7226 (1987).

[22] I. Felner, I. Nowik, and Y. Yeshurun, Phys. Rev. B **36**, 3923 (1987).

[23] R. C. Sherwood, S. Jin, T. H. Tiefel, R. B. Van Dover, R. A. Fastnacht, M. F. Yan, and W. W. Rhodes, in Ref. 13, p. 503.

[24] Y. K. Tao, J. S. Swinnea, A. Manthiram, J. S. Kim, J. B. Goodenough, and H. Steinfink, in Ref. 13, p. 519.

[25] C. U. Segre, C. W. Kimball, A. E. Dwight, B. D. Dunlap, J. D. Jorgensen, and B. W. Veal, Bull. Am. Phys. Soc. **33**, 347 (1988).

[26] J. R. Ashburn, C. A. Higgins, A. Hampton, and M. K. Wu, Bull. Am. Phys. Soc. **33**, 348 (1988).

[27] Y. Xu, A. R. Moodenbaugh, R. L. Sabatini, and M. Suenaga, in *High Temperature Superconductors II,* edited by D. W. Capone II, W. H. Butler, B. Batlogg, and C. W. Chu, Materials Research Society Symposia Proceedings (Materials Research Society, Pittsburgh, 1988), EA-14, p. 373.

[28] Y. Xu, R. L. Sabatini, A. R. Moodenbaugh, and M. Suenaga, Phys. Rev. B **38**, 7084 (1988).

[29] K. Sasaki, K. Fujii, K. Kuroda, H. Saka, and T. Imura, in Proceedings of the International Conference on New Materials, Tokyo, March 1988 (unpublished).

[30] T. Ichihashi, S. Iijima, Y. Kubo, Y. Shinakawa, and J. Tabuchi, Jpn. J. Appl. Phys. **27**, L594 (1988).

[31] H. M. Rietveld, J. Appl. Crystallogr. **2**, 65 (1969).

[32] A. W. Hewat, Atomic Energy Research Establishment, Harwell, Berkshire, United Kingdom, Report No. R7350, 1973 (unpublished).

[33] P. Zolliker, D. E. Cox, J. M. Tranquada, and G. Shirane, Phys. Rev. B **38**, 6575 (1988).

[34] H. G. Scott, J. Appl. Cryst. **16**, 159 (1983).

[35] L. Koester and H. Rauch, International Atomic Energy Agency, Vienna, Report No. 2517/Rb, 1981 (unpublished).

[36] J. M. Tranquada, D. E. Cox, W. Kunnmann, H. Moudden, G. Shirane, M. Suenaga, P. Zolliker, D. Vaknin, S. K. Sinha, M. S. Alvarez, A. J. Jacobson, and D. C. Johnston, Phys. Rev. Lett. **60**, 156 (1988); J. M. Tranquada, A. H. Moudden, A. I. Goldman, P. Zolliker, D. E. Cox, G. Shirane, S. K. Sinha, D. Vaknin, D. C. Johnston, M. S. Alvarez, A. J. Jacobson, J. T. Lewandowski, and J. M. Newsam, Phys. Rev. B **38**, 2477 (1988).

[37] A. A. Abrikosov and L. P. Gor'kov, Zh. Eksp. Teor. Fiz. **39**, 1781 (1961) [Sov. Phys. JETP **12**, 1243 (1961)].

[38] S. Noguch, J. Inoue, K. Okuda, Y. Maeno, and T. Tujita, Jpn. J. Appl. Phys. **27**, L390 (1988).

[39] See, for example, J. Electron. Microsc. Technol. **8**, (1988). This issue is devoted to microscopy of $YBa_2Cu_3O_{7-\delta}$.

[40] Y. Zhu, M. Suenaga, Y. Xu, R. L. Sabatini, and A. R. Moodenbaugh (unpublished).

[41] P. Bordet, J. L. Hodeau, P. Strobel, M. Marezio, and A. Santoro, Solid State Commun. **66**, 435 (1988).

[42] M. A. Alario-Franco, C. Chaillout, J. J. Capponi, and J. Chenavas, Mater. Res. Bull. **23**, 313 (1988).

[43] J. Tafto (unpublished).

[44] M. Sarikaya, R. Kikuchi, and I. A. Aksay, Physica C **152**, 161 (1988); M. Sarikaya and E. Stern, Phys. Rev. B **37**, 9373 (1988).

[45] C. J. Barry, J. Electron. Microsc. Technol. **8**, 325 (1988).

[46] D. O. Welch (unpublished).

[47] G. Arlt and P. Sasko, J. Appl. Phys. **51**, 4956 (1980).

[48] T. M. Shaw, S. L. Shinde, D. Dimos, R. F. Cook, P. R. Duncombe, and C. Kroll, J. Mater. Res. **3**, 1297 (1988).

[49] L. S. Chumbey, J. D. Verhoeven, M. R. Kim, A. L. Corneliu, and M. J. Kramer, IEEE Trans. Magn. (to be published).

[50] N. Chandraseker, D. O. Welch, and M. Suenaga (unpublished).

[51] H. W. Zandbergen, G. van Tendeloo, T. Okabe, and S. Amelinckx, Phys. Status Solidi A **103**, 45 (1987).

[52] S. Iijima, T. Ichihashi, Y. Kubo, and J. Tabuchi, Jpn. J. Appl. Phys. **26**, L1790 (1987).

[53] Z. Hiroi, M. Takano, Y. Takeda, R. Kanno, and Y. Bando, Jpn. J. Appl. Phys. **27**, L580 (1988).

[54] G. Roth, G. Heger, B. Renker, J. Pannetier, V. Caignaert, M. Herrieu, and B. Raveau, Z. Phys. B **71**, 43 (1988).

[55] G. van Tendeloo and S. Amelinckx, J. Electron. Microsc. Technol. **8**, 285 (1988).

[56] G. V. S. Sastry, R. Wördenweber, and H. Freyhardt (unpublished).

[57] Y. Zhu (unpublished).

[58] A. W. Sleight, in Ref. 13, p. 3.

[59] P. F. Miceli, J. M. Tarascon, L. H. Greene, P. Barboux, F. J. Rotella, and J. D. Jorgensen, Phys. Rev. B **37**, 5932 (1988).

[60] N. Okazaki, S. Kambe, A. Kishi, N. Kanazawa, A. Ohtomo, A. Fukuoka, T. Hasegawa, K. Kishio, K. Kitazawa, and K. Fueki (unpublished).

[61] J. M. Tranquada, S. M. Heald, A. R. Moodenbaugh, and Youwen Xu, Phys. Rev. B **38**, 8893 (1988).

[62] M. Murakami, S. Matsuda, H. Teshima, M. Morita, and M. Nagumo (unpublished).

[63] P. H. Kes, Physica C **153-155**, 1121 (1988).

[64] T. Matsushita, K. Fumaki, M. Tako, and K. Yamafuji, Jpn. J. Appl. Phys. **26**, L1524 (1987).

[65] R. Wördenweber, G. V. S. Sastray, K. Hieneman, and H. C. Freyhardt, J. Appl. Phys. **65**, 1648 (1989).

[66] S. T. Sekula, J. Brynestad, D. K. Kristen, J. R. Thompson, and Y. Kim, IEEE Trans. Magn. (to be published).

[67] D. K. Finnemore, K. Athreya, S. Sanders, Y. Xu, and M. Suenaga (unpublished).

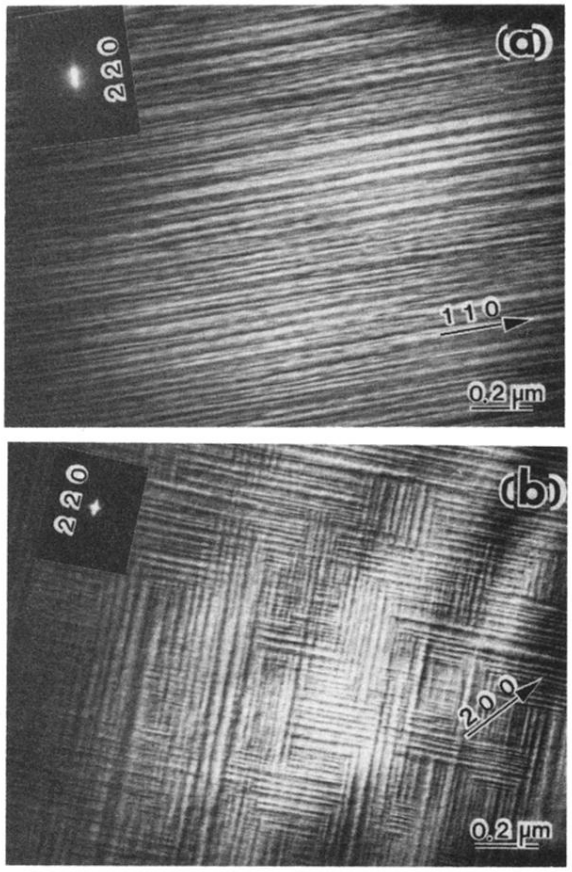

FIG. 10. Dark-field transmission electron micrographs of $YBa_2(Cu_{0.98}Fe_{0.02})_3O_{7-\delta}$ showing very finely divided twins from two different areas using $g=\langle 200\rangle$ to image the twins in both directions. The insets show appearance of very weak diffuse scattering streaks along the $\langle hh0\rangle$ and $\langle \bar{h}h0\rangle$ directions.

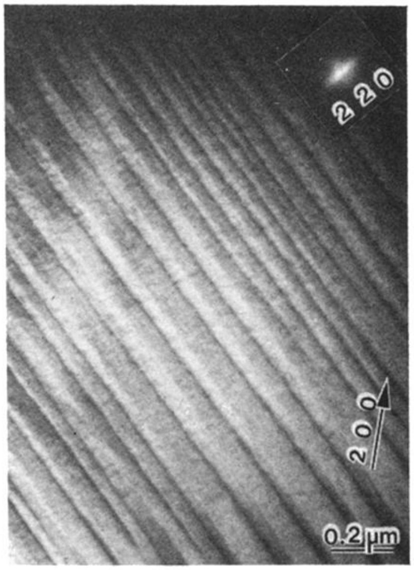

FIG. 11. A dark-field transmission electron micrograph of $YBa_2(Cu_{0.975}Fe_{0.025})_3O_{7-\delta}$ showing the twins and the tweed structure which are superimposed. The diffraction condition was $\langle 200\rangle$ to show the tweed in both of the $\langle hh0\rangle$ directions. The inset shows the reduced separation of the $\langle 220\rangle$ split and the increased intensity on the diffuse scattering streak.

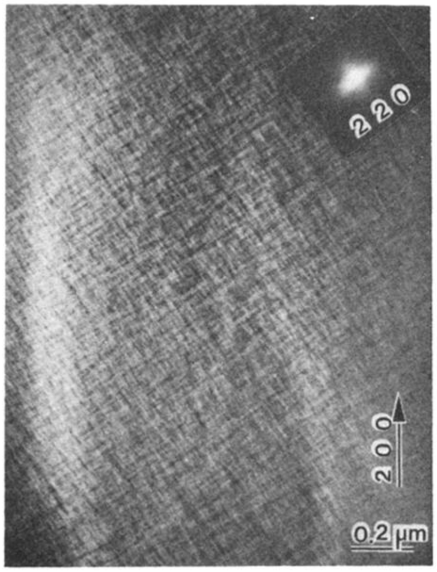

FIG. 12. A dark-field transmission electron micrograph of $YBa_2(Cu_{0.97}Fe_{0.03})_3O_{7-\delta}$ showing the tweedlike structure using $g=\langle 200\rangle$. Note that the $\langle 220\rangle$ reflection is not split and the diffuse scattering is stronger than that for $x \lesssim 0.025$.

FIG. 13. A ⟨001⟩ zone selected area electron-diffraction pattern form the area in Fig. 12 showing the crossed diffuse scattering at all ⟨*hk*0⟩ diffraction.

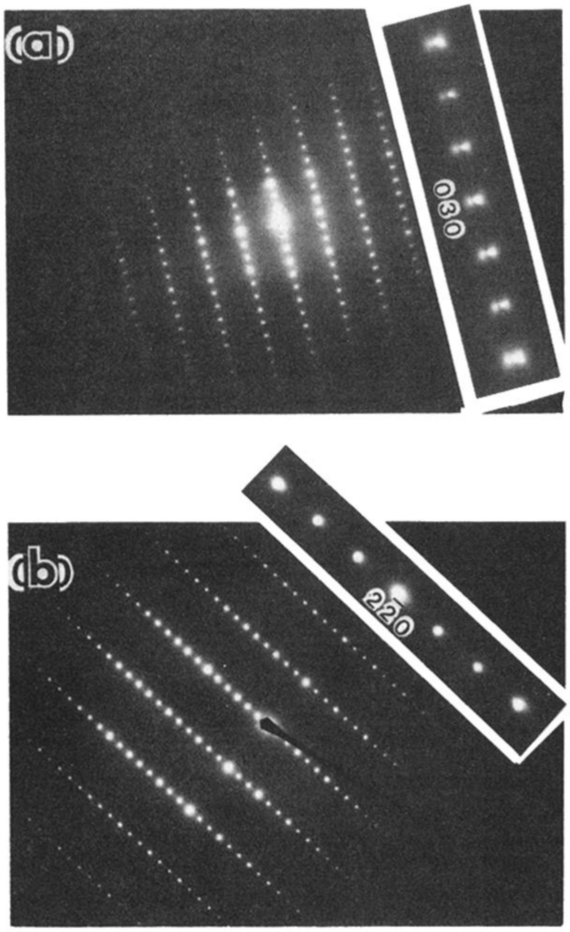

FIG. 14. Selected area electron-diffraction patterns from (a) the ⟨100⟩ and (b) the ⟨110⟩ zones of $YBa_2(Cu_{0.97}Fe_{0.03})_3O_{7-\delta}$. The insets show (a) the presence of and (b) the absence of the diffuse scattering in the ⟨100⟩ and the ⟨110⟩ zones, respectively.

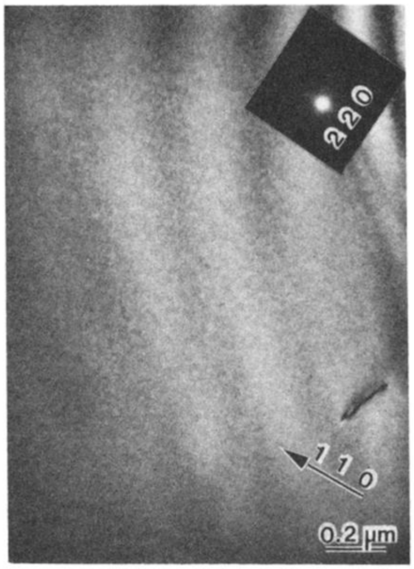

FIG. 15. A dark-field transmission electron micrograph from $YBa_2(Cu_{0.90}Fe_{0.10})_3O_{7-\delta}$. At this composition, the tweedlike structure is not clearly visible but weak diffuse streaks exist (see inset) $g = \langle 200 \rangle$.

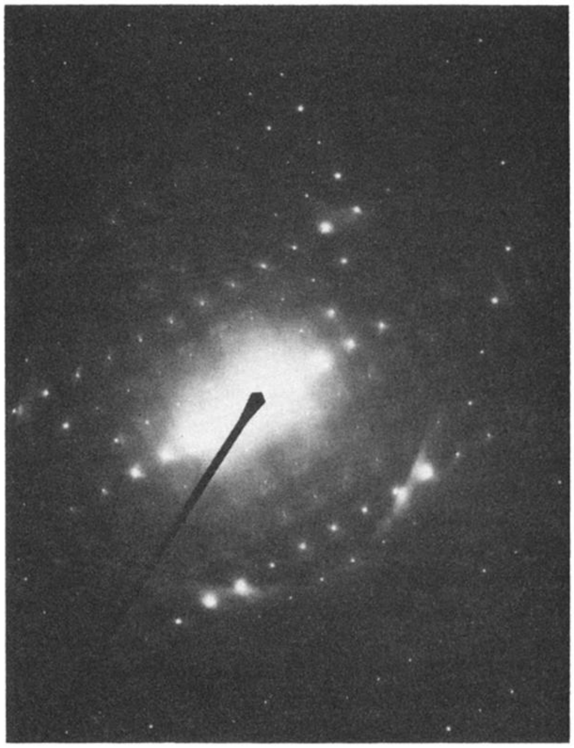

FIG. 16. A selected area diffraction from $YBa_2(Cu_{0.85}Fe_{0.15})_3O_{7-\delta}$ showing the appearance of diffuse scattering which is centered at a position along the ⟨*hh*0⟩ direction and at $0.167(\sqrt{2}/a)$. The electron-diffraction pattern is taken by tilting ~15° away from the ⟨001⟩ zone along the [*hh*0] direction.

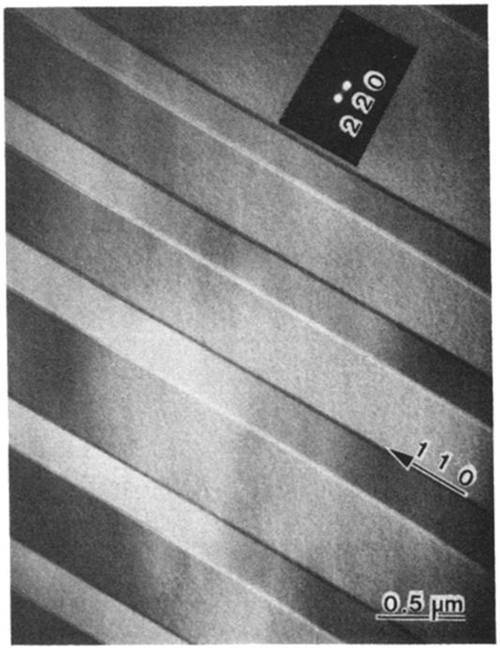

FIG. 7. A dark-field transmission electron micrograph of a $YBa_2Cu_3O_7$ taken with $g = \langle 110 \rangle$ showing very large twins. The inset indicates the degree of the split at the $\langle 220 \rangle$ reflection due to the twin formation. In this case g is parallel to the twin boundary and the direction of the split is perpendicular to the boundary and g.

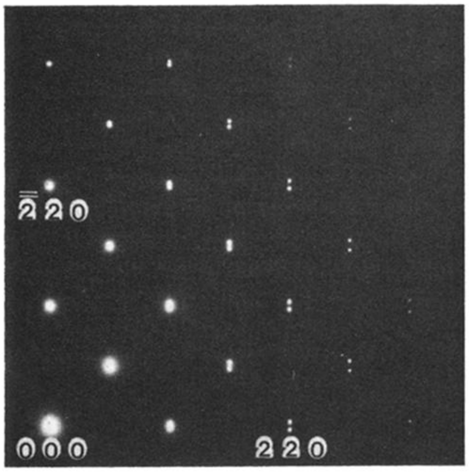

FIG. 8. A selected area electron-diffraction pattern from the area shown in Fig. 6. Note that the twin boundary is parallel to the $[hh0]$ direction and the split at the diffraction spots is zero at the $[\bar{h}h0]$ and maximum at the $[hh0]$.

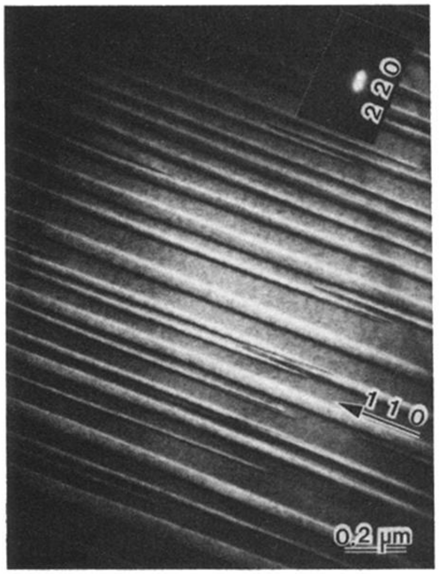

FIG. 9. A dark-field transmission electron micrograph of $YBa_2(Cu_{0.985}Fe_{0.015})_3O_{7-\delta}$ taken with $g = \langle 110 \rangle$. Note that the size of the twins and the separation of the $\langle 220 \rangle$ spots are significantly reduced.